Journal of
**Synchrotron
Radiation**

ISSN 0909-0495

Received 18 December 2012
Accepted 2 May 2013

Accuracy evaluation in temperature-dependent EXAFS measurements of CdTe

N. Abd el All,[a,b] B. Thiodjio Sendja,[c,d] R. Grisenti,[a] F. Rocca,[e] D. Diop,[d] O. Mathon,[f] S. Pascarelli[f] and P. Fornasini[a]*

[a]Dipartimento di Fisica, Università di Trento, I-38123 Povo (Trento), Italy, [b]Physics Department, Assiut University, Assiut, Egypt, [c]Ecole Nationale Supérieure Polytechnique, University of Yaoundé, PO Box 8390, Yaoundé, Cameroon, [d]Départment de Physique, Université Cheick Anta Diop, Dakar, Senegal, [e]IFN-CNR, Istituto di Fotonica e Nanotecnologie, Unità 'FBK-Fotonica' di Trento, I-38123 Povo (Trento), Italy, and [f]ESRF, Grenoble, France. E-mail: paolo.fornasini@unitn.it

The evaluation of uncertainty in temperature-dependent EXAFS measurements is discussed, considering the specific case of a recent experiment performed on CdTe. EXAFS at both Cd and Te *K*-edges was measured at different times and at different beamlines in a temperature range from 5 to 300 K. Attention is focused on the nearest-neighbours parameters: bond thermal expansion, parallel and perpendicular mean-square relative displacements and the third cumulant. Different causes of uncertainty, a comparison of experimental results with theoretical models, the difference between EXAFS and crystallographic thermal expansions and the meaning of the third cumulant are discussed.

Keywords: EXAFS; thermal expansion; mean-square relative displacements; Einstein model; Debye model.

1. Introduction

The widespread use of EXAFS as a structural tool by a large number of researchers belonging to different research fields and with different scientific backgrounds, accompanied by a spread of quality levels of published papers, stimulates the effort to develop effective standardization criteria (Ascone *et al.*, 2012). A key step towards standardization is the agreement on the methods for evaluating and possibly increasing the accuracy of structural parameters obtained from EXAFS. A sound evaluation of accuracy, necessary to guarantee the reliability of results and to avoid incorrect interpretations, is generally far from trivial, since it requires a careful investigation of the various sources of errors and uncertainties in both experimental activity and data analysis procedure.

In the last few years a fundamental contribution has been given by Chantler and co-workers, who developed a suite of experimental techniques and procedures (the so-called X-ray extended-range technique, XERT) for the accurate measurement of the X-ray mass attenuation coefficient (Chantler *et al.*, 2001, 2012*a*,*b*). Recently, the accuracy of the absolute values of structural parameters from EXAFS has been addressed too (Glover *et al.*, 2010).

One can expect that a wider application of XERT, or of similar approaches, to selected model compounds contributes to the calibration of EXAFS measurement methods. On the other hand, XERT is still far from a standard routine method and its extension to most of the typical EXAFS experiments, for which a reasonable compromise has to be found between the complexity of samples, the extent of new sought information, the accuracy of the results and the available synchrotron radiation beam time, seems at present to be out of the question. Besides, a good deal of actual EXAFS experiments aim at seeking relative values of structural parameters (*e.g.* as a function of temperature or pressure), and can achieve higher accuracy than absolute measurements with less stringent requirements for both experimental set-ups and data analysis procedures.

Accuracy of the order of the femtometer was obtained for the distance variation caused by magnetostriction in an iron–cobalt thin film, by means of an X-ray-dispersive spectrometer (Pettifer *et al.*, 2005). The possibility of detecting differences in interatomic distances of the order of 10 fm by a conventional transmission apparatus was demonstrated by the measurement of isotopic effects in the Debye–Waller factor and in the thermal expansion of the germanium first shell (Purans *et al.*, 2008). Differences of a few 10 fm are routinely detected in bond thermal expansion studies and have allowed the measurement of the difference between bond and lattice thermal expansions (Fornasini *et al.*, 2004; Abd el All *et al.*, 2012) as well as the study of the anomalously small thermal expansion of Invar alloys (Yokoyama & Eguchi, 2011).

A thorough investigation of the accuracy attainable in relative EXAFS measurements performed on standard synchrotron radiation beamlines to solve a realistic scientific problem may be helpful to many EXAFS practitioners and contribute to the debate on the improvement of experimental data quality. This kind of bottom-up approach should be

doi:10.1107/S0909049513012053

considered as complementary to and not substitutive of the top-down approach of XERT. Within this framework we discuss here in some detail the evaluation of the accuracy in a recent study of the temperature dependence of EXAFS of CdTe (Abd el All *et al.*, 2012). The main aim of that experiment was to investigate the local dynamical behaviour of CdTe, in terms of bond thermal expansion and parallel and perpendicular mean-square relative displacements (MSRDs), and to compare it with the average dynamical behaviour, characterized by a lattice thermal expansion that is negative at low temperatures and positive at high temperatures.

The experiment performed on CdTe is particularly suited for the present investigation on the origin and extent of uncertainties and errors. The measurements were performed at the two edges of Cd and Te at different times and at different beamlines; the data analysis was independently carried on by different researchers; for the first-shell analysis, two intrinsically different procedures were used and compared, the ratio method and the non-linear fit to theoretical simulations.

We focus our attention here on the results obtained for the nearest-neighbour Cd–Te distance, for which a better resolution and accuracy of bond thermal expansion can be achieved with respect to the outer shells. The experimental details are discussed in §2. §3 is dedicated to a critical appraisal of the data analysis. The main results, consisting of the temperature dependence of the first four cumulants, are presented in §4. In §5 the discussion is focused on the evaluation of uncertainty, on the comparison of experimental data with theoretical models, on the difference between EXAFS and crystallographic distances and on the meaning of the third cumulant. §6 is dedicated to conclusions.

2. Experimental considerations

Transmission EXAFS measurements have been performed at ESRF, Grenoble, on CdTe powders, 99.999% pure. EXAFS at the Cd *K*-edge was measured at the ESRF-BM29 beamline in 2008. EXAFS at the Te *K*-edge was measured at the ESRF-BM23 beamline in 2011. The BM23 beamline is actually an upgrade of BM29: the two beamlines basically differ with regard to the location of the emitting bending magnet along the storage ring, some mechanical details of the monochromator assembly and the cryostat. The storage ring electron energy and average current were 6 GeV and about 190 mA, respectively, for both experiments.

2.1. Sample homogeneity

Two different samples had been prepared for the two sets of measurements (Cd and Te edges) by precipitating the CdTe powders on polytetraflouroethylene membranes from suspensions in methyl alcohol. The samples' homogeneity was checked by measuring the intensity of the transmitted photon beam as a function of the vertical and horizontal position. The EXAFS measurement position was chosen in the middle of a region where the transmitted intensity was constant. The size of the beam incident on the sample was about 4 mm × 1 mm and 1 mm × 1 mm for the Cd *K*-edge and the Te *K*-edge measurements, respectively. The edge jump $\Delta\mu x$ was about 1.0 and about 0.8 for the Cd *K*-edge and the Te *K*-edge, respectively. The impinging position of the beam on the samples was re-calibrated after each temperature variation. The spread of the edge jump values for different spectra at different temperatures was within 4% and 2% for the Cd and Te samples, respectively.

2.2. Photon energy

In both experiments the X-ray beam was monochromatized by two silicon crystals with flat (311) parallel reflecting faces ($2d$ = 3.17404 Å), thermalized at a temperature of 110 K, where the thermal expansion coefficient of silicon is $|\alpha| \leq 15 \times 10^{-6}\,\mathrm{K}^{-1}$. The relative influence of harmonics was reduced below 10^{-5} by total reflection from two Pt-coated mirrors (incidence angle 2 mrad). The X-ray energy was scanned in the ranges E = 26400–28230 eV (for Cd) and E = 31500–33800 eV (for Te), with the ΔE step varying from 0.5 eV in the near-edge region to 5 eV at the end of the spectra, in order to obtain a uniform wavevector step Δk = 0.025 Å in the EXAFS region. There was no detuning of the two monochromator crystals, one always worked at the maximum of the rocking curve using feedback based on a lock-in amplifier (Prestipino *et al.*, 2011).

According to the Bragg law the variations of the monochromator temperature T influence the X-rays energy as

$$\Delta E = E\,\alpha\,\Delta T, \tag{1}$$

and the relation between Bragg angle variations and energy variations is

$$\Delta E = E\,\Delta\theta\,/\tan\theta\,. \tag{2}$$

Equation (2) accounts both for the spread of the angular values (owing to source size, slits apertures, monochromator Darwin width), which contributes to the energy resolution, and for the shift of the angular position, which reflects the shift of the energy axis. The energy resolution was estimated at about 5 eV for Cd and 7 eV for Te, smaller than the respective core level widths. The shift of the energy axis is discussed below, in §3.

The incoming and outgoing photon fluxes were measured by two ionization chambers filled with krypton gas, at respective pressures of 140 and 500 mbar. The total flux incident on the samples was estimated to be of the order of a few 10^9 photons s^{-1} for both experiments.

2.3. Temperature

For the Cd *K*-edge EXAFS, the temperature was varied from 19 to 300 K, in 25 K steps below 150 K and in 50 K steps above 150 K, using a helium gas flow cryostat. For the Te *K*-edge EXAFS, the temperature was varied from 4 to 300 K in 10 K steps below 100 K and in 25 K steps above 100 K, using a liquid-helium cryostat (Steinmann & van der Linden, 2006). The sample was pressed between the two plates of the sample holder, which was in turn fixed to the cryostat cold head by a M4 bronze screw, screwed with a torque of at least 1 N m. Both sample holder and cold head were gold plated with a 5 µm-thick layer. The temperature difference between the cold head and the sample was less than 1 K. The power load owing to the beam was well below 1 mW. The temperature uncertainty of measurements was evaluated to be no larger than 1 K. The reliability of the temperature scales has been *a posteriori* checked by the agreement with theoretical expectations of the temperature dependence of the leading cumulants, in particular of the second one (the EXAFS Debye–Waller factor), as well as by the good agreement between the results from Cd and Te edges.

A minimum of two and a maximum of five spectra were recorded at each temperature, to allow a reasonable evaluation of the experimental uncertainty (see below).

3. Data analysis

The data analysis procedure has been summarized by Abd el All *et al.* (2012). Here we focus our attention on the issues most relevant to the accuracy evaluation.

3.1. Extraction of the EXAFS signal

The extraction of the EXAFS signals $\chi(k)$ from the experimental spectra was performed according to a well established procedure (Vaccari *et al.*, 2007). A straight line best fitting the pre-edge signal was preliminarily subtracted from the spectra.

For each of the two sets of measurements (Cd and Te edges) the values of the photoelectron wavevector k were calculated with respect to an edge energy E_s, conventionally set at the maximum of the first derivative of one of the spectra, chosen as reference. The energy axes of all other spectra were then shifted to achieve the best superposition with the reference spectrum in the edge region, and the edge energy E_s of each spectrum was determined accordingly. No variation of the edge shape was observed as a function of temperature.

The variation of the nominal edge position E_s with respect to the real edge position is a good test of the energy axis stability; ideally it should be zero. Fig. 1 shows the variation with time of the E_s values for the Cd K-edge. The spread of E_s values is smaller than the 0.5 eV acquisition step. The overall variation is too large to be attributed to temperature effects on the monochromator planar spacing [equation (1)]. From equation (2), for the Cd K-edge one finds $\Delta E\,[\text{eV}] \simeq 1.85 \times 10^5 \Delta\theta\,[\text{rad}]$. It is reasonable to attribute the edge energy shift to a variation of the monochromator Bragg angle, caused by long-period instabilities of the beam and mechanical and thermal instabilities of the different components of the optical apparatus.

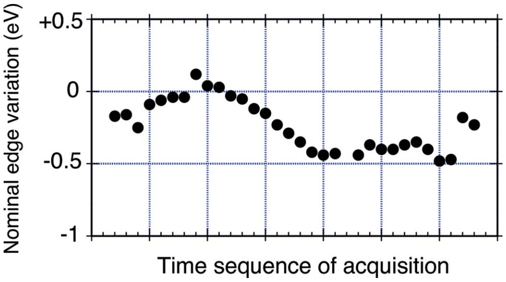

Figure 1
Variation of the nominal Cd K-edge position as a function of time. Each point corresponds to a spectrum corresponding to 50 min of acquisition time.

From Fig. 1 one can infer that the maximum energy shift during the acquisition of a single spectrum is about 0.05 eV. Such a shift, distributed along the 1500 eV range of an EXAFS signal, would correspond to a stretch of the wavevector k axis leading to an error of about 5×10^{-5} Å for the nearest-neighbours distance of 2.8 Å.

The EXAFS signal was obtained as $\chi(k) = (\mu - \mu_1)/\mu_0$, where μ is the experimental absorption coefficient, μ_1 is a spline polynomial best fitting the average behaviour of μ, and μ_0 is a Victoreen-type function with absolute values normalized to the experimental absorption jump of the spectra. This choice was made to minimize the effects of the difference in the average behaviour of different files at high energy. The alternative choice, $\chi(k) = (\mu - \mu_1)/\mu_1$ (denominator equal to the best-fitting spline), was checked in any case. The differences between the two procedures on the final values amount to 3×10^{-5} Å for the first cumulant, 1×10^{-5} Å^2 for the second cumulant and less than 10^{-7} Å^3 for the third cumulant, significantly smaller than the discrepancies between different files at the same temperature. A good agreement was found also with the relative values of cumulants obtained using the normalization procedure 'autobk' of the *Athena* package (Ravel & Newville, 2005). Examples of $k^2\chi(k)$ functions are shown in Fig. 2.

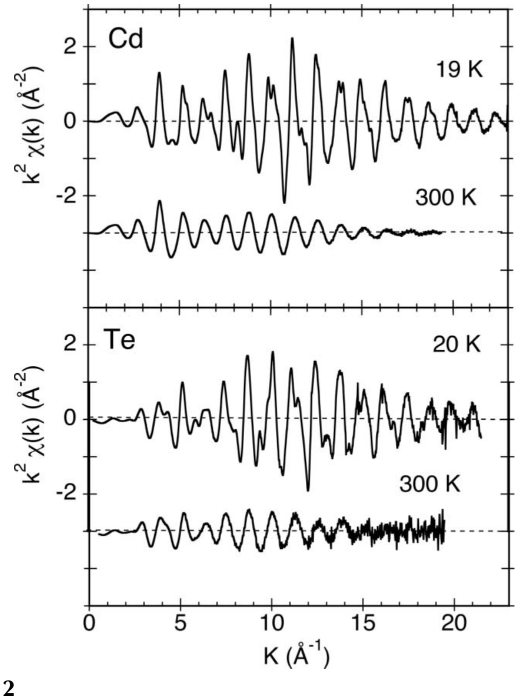

Figure 2
EXAFS signals $k^2\chi(k)$ at the K-edges of Cd (top) and Te (bottom) at selected temperatures.

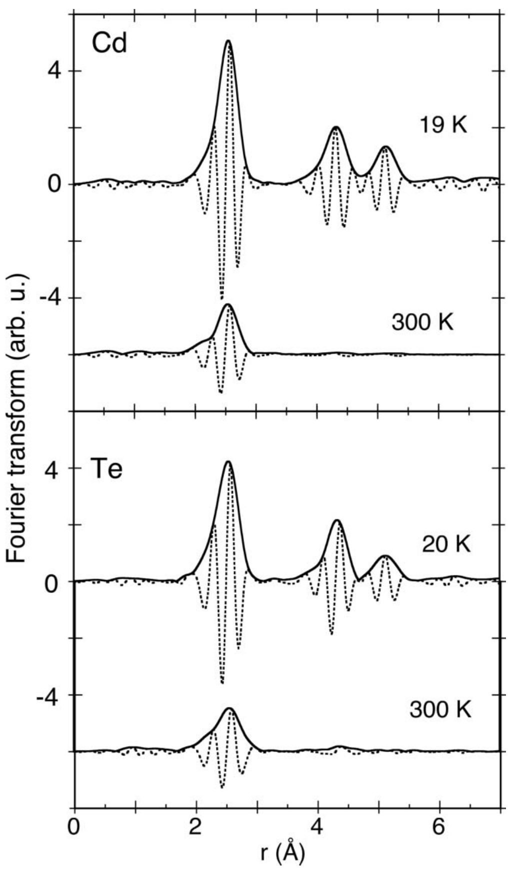

Figure 3
Fourier transforms of the EXAFS signals at the *K*-edges of Cd (top) and Te (bottom) at selected temperatures.

The *k*-weighted EXAFS signals $k^2\chi(k)$ were Fourier transformed from $k_{\rm min}$ = 1.8 to $k_{\rm max}$ = 19 Å^{-1}, after multiplication by a Gaussian function whose amplitude at the extrema of the wavevector interval was 10% of the amplitude at the centre.

The Fourier transforms at selected temperatures are shown in Fig. 3. The peak due to the nearest-neighbours single-scattering contribution (four atoms at 2.8 Å) appears well isolated at all temperatures. Only the quantitative analysis of the first-shell contribution is considered here. To that purpose, the corresponding signal in real space (from 1.6 to 3.2 Å in Fig. 3) was back-transformed to *k* space. The possible leakage of longer scattering paths on the first-shell contribution has been checked (see below).

3.2. Quantitative analysis

As in previous works (Fornasini *et al.*, 2004; Vaccari *et al.*, 2007), quantitative results for the first shell have been obtained by both the ratio method and the non-linear fit of calculated to experimental spectra. A partial discussion of the relative merits of the two procedures has been made by Vaccari *et al.* (2007).

3.2.1. Ratio method. The ratio method (Bunker, 1983; Dalba *et al.*, 1993) consists of the separate analysis of phase and amplitude of the EXAFS signal at each temperature, taking a low-temperature spectrum as reference. The ratio method is well suited to accurate studies of the variations of first-shell parameters induced by temperature or pressure variations, because it does not require theoretical inputs and allows a direct, though quite conservative, visual estimate of the quality of data. Moreover, it avoids the statistical correlation between even and odd cumulants which can instead affect the non-linear fitting procedures (the correlation introduced by the Fourier filtering procedure cannot be disentangled).

For each of the two sets of measurements (Cd and Te edges), the first-shell EXAFS signals were obtained by Fourier back-transforming the corresponding peak in real space. Phases and amplitudes of the filtered signals at the different temperatures (*s*) were then compared with the phase and amplitude of the average of the signals at 19 K (Cd *K*-edge) or 20 K (Te *K*-edge), taken as reference (*r*).

In principle, the ratio method is sensitive to the relative values $\delta C_n = C_{n,s} - C_{n,r}$ of the cumulants of an effective distribution $P(r,\lambda) = \rho(r)\exp(-2r/\lambda)/r^2$, where $\rho(r)$ is the real distribution of distances and λ is the photoelectron mean free path.

If the logarithm of the amplitude ratios is plotted against k^2 (Fig. 4), the linear slope is proportional to the difference of the second cumulants $\delta C_2 = C_{2,s} - C_{2,r}$, and the difference of the fourth cumulants $\delta C_4 = C_{4,s} - C_{4,r}$ is reflected in a slight deviation from linearity. The plot allows a visual evaluation of the quality of signals: different files at the same temperature should give the same plot; the spread with respect to the average behaviour is a measure of uncertainty, and the fitting interval has been chosen as the interval where the different files at the same temperature have a reasonably similar behaviour (for example, below k^2 = 200 Å^{-2} in Fig. 4). Note that the logarithm strongly enhances the differences at high *k* values, where the amplitudes are smaller and the signal-to-noise ratio becomes critical.

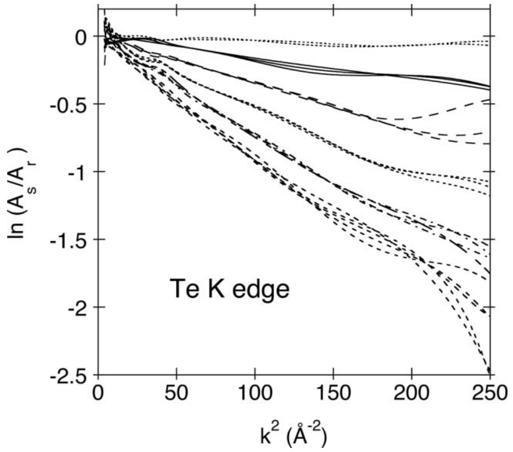

Figure 4
Logarithms of amplitude ratios plotted against k^2 for some EXAFS spectra at the Te *K*-edge. The reference *r* is the average of the spectra measured at 20 K. The different bundles of lines refer to the signals *s* at (in order of increasing slope) 50, 100, 150, 200, 250 and 300 K.

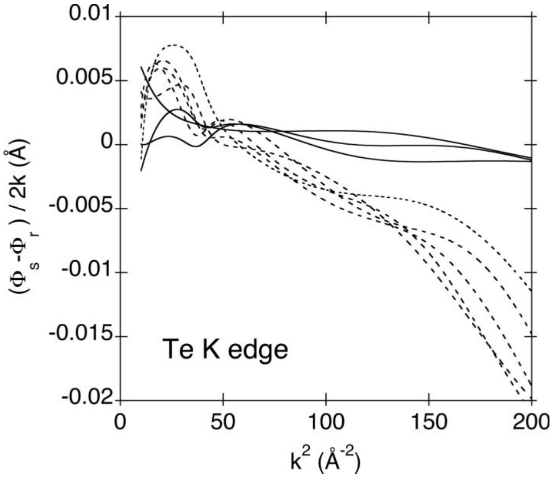

Figure 5
Difference of phases divided by $2k$ plotted against k^2 for the EXAFS spectra at the Te *K*-edge. The reference *r* is the average of the spectra measured at 20 K. The bundles of continuous and dashed lines refer to the signals *s* at 100 K and 300 K, respectively.

If the difference of phases divided by $2k$ is plotted against k^2 (Fig. 5), the vertical intercept gives the difference of the first cumulants $\delta C_1 = C_{1,s} - C_{1,r}$ and the linear slope is proportional to the difference of the third cumulants $\delta C_3 = C_{3,s} - C_{3,r}$. Again, the plot allows a visual evaluation of the quality of signals. In general, the quality of signals is more critical for phase plots than for amplitude plots: the spread of the different files at a given temperature with respect to the average behaviour is larger than for amplitudes, and the choice of the fitting interval requires particular care. The spread is particularly evident not only at high k^2 values, where the signal-to-noise ratio is poorer, but also at low k^2 values, where the differences introduced by the procedure of background subtraction are boosted by the $1/k$ factor in the vertical axis. Also for the phase analysis, the fitting interval has been chosen as the interval where the different files at the same temperature have a reasonably similar behaviour.

The fitting procedure substitutes the cumulant series by finite polynomials. From the ratio method one obtains the relative values of a few polynomial coefficients $\delta\tilde{C}_n$, typically $n \leq 4$. The correspondence between the polynomial coefficients $\delta\tilde{C}_n$ and the leading cumulants δC_n of the effective distribution depends on the convergence properties of the cumulant series. This issue has been experimentally investigated by Crozier *et al.* (1988) and Dalba *et al.* (1993). In the present case of CdTe, the adequacy of the polynomial coefficients was *a posteriori* confirmed by their temperature dependence (see below).

The evaluation of the uncertainties on the relative values of cumulants was performed, independently for the Cd and Te edges, according to the following procedure.

(i) As a first step, the spectra measured at the reference temperature (19 K for Cd, 20 K for Te) were averaged, to obtain a unique reference spectrum; the comparison of the different spectra at the reference temperature with their average spectrum represents a good test of short-term reproducibility. The relative cumulant values from different spectra were considered as the results of independent measurements, sampling a Gaussian population, and their uncertainty estimated as the standard deviation of the mean: $\sigma(\delta C_1) \simeq 2 \times 10^{-4}$ Å, $\sigma(\delta C_2) \simeq 2 \times 10^{-5}$ Å^2, $\sigma(\delta C_3) \simeq 1 \times 10^{-6}$ Å^3.

Table 1
Relative values of the first cumulants of the effective distribution and of the first three cumulants of the real distribution of nearest-neighbours distances and corresponding evaluated uncertainties at selected temperatures for the Te *K*-edge.

	δC_1 (10^{-2} Å)	δC_1^* (10^{-2} Å)	δC_2^* (10^{-2} Å^2)	δC_3^* (10^{-4} Å^3)
100 K	0.187 ± 0.06	0.265 ± 0.07	0.089 ± 0.006	0.21 ± 0.04
200 K	0.448 ± 0.06	0.713 ± 0.07	0.281 ± 0.003	0.79 ± 0.1
300 K	0.704 ± 0.06	1.17 ± 0.07	0.45 ± 0.005	1.6 ± 0.18

(ii) At each temperature, all the spectra were compared with the average reference spectrum; different fitting ranges in k space were attempted for both phases and amplitudes, within k intervals where the curves of different spectra shared a reasonably regular behaviour. Typical intervals ranged from $k_{\min} = 4$ to $k_{\max} = 13$–15 Å^{-1}. Again, the relative cumulant values from different spectra for the same fitting interval were considered as the results of independent measurements, sampling a Gaussian population, and their uncertainty was estimated as the standard deviation of the mean. The values from different fitting intervals were considered as sampling a uniform distribution, and the corresponding uncertainty was estimated as the standard deviation of the rectangular distribution, $\Delta(\delta C_n)/(12)^{1/2}$ (Fornasini, 2008).

(iii) The total uncertainty of the relative values δC_n of the cumulants at a given temperature was obtained by the quadratic sum of the three contributions: reference, different spectra and different fitting intervals.

At the end of the procedure of data analysis by the ratio method, the cumulants of the real distribution, C_n^*, were calculated from the cumulants of the effective distribution, C_n, according to the recursion formula (Vaccari *et al.*, 2007),

$$C_n^* \simeq C_n + 2C_{n+1}(1/C_1 + 1/\lambda) \quad \text{for } n = 1, 2, 3. \qquad (3)$$

Since the ratio method cannot take into account the k dependence of the electron mean free path $\lambda(k)$, three different constant values λ = 6, 9, 12 Å were used in (3). The corresponding uncertainty, evaluated as the standard deviation of a rectangular distribution, was quadratically summed to the uncertainty of the effective relative cumulants δC_n to obtain the uncertainty of the real relative cumulants δC_n^*. The difference between the cumulants of the real and effective distributions is significant only for the first cumulant (average distance).

As an example of uncertainty evaluation, the relative values of the cumulants from Te *K* EXAFS are shown in Table 1 for selected temperatures.

One can see that the uncertainty caused by the loose assumption on the mean free path only slightly increases the uncertainty of the first real cumulant δC_1^* ($\sim$0.07 × 10^{-2} Å)

Table 2

Comparison of the main parameters obtained from the Cd and Te EXAFS analyses: best-fitting Einstein frequencies for the parallel and perpendicular MSRDs, third-order force constant and zero point value of the third cumulant.

	Cd *K*-edge	Te *K*-edge
$\nu_\parallel$ (THz)	3.9 ± 0.03	3.88 ± 0.005
$\nu_\perp$ (THz)	1.84 ± 0.02	1.82 ± 0.02
k_3 (eV Å^{-3})	-1.92 ± 0.03	-2.07 ± 0.03
C_3^* at 0 K (Å^3)	$(0.33 \pm 0.05) \times 10^{-5}$	$(0.42 \pm 0.04) \times 10^{-5}$

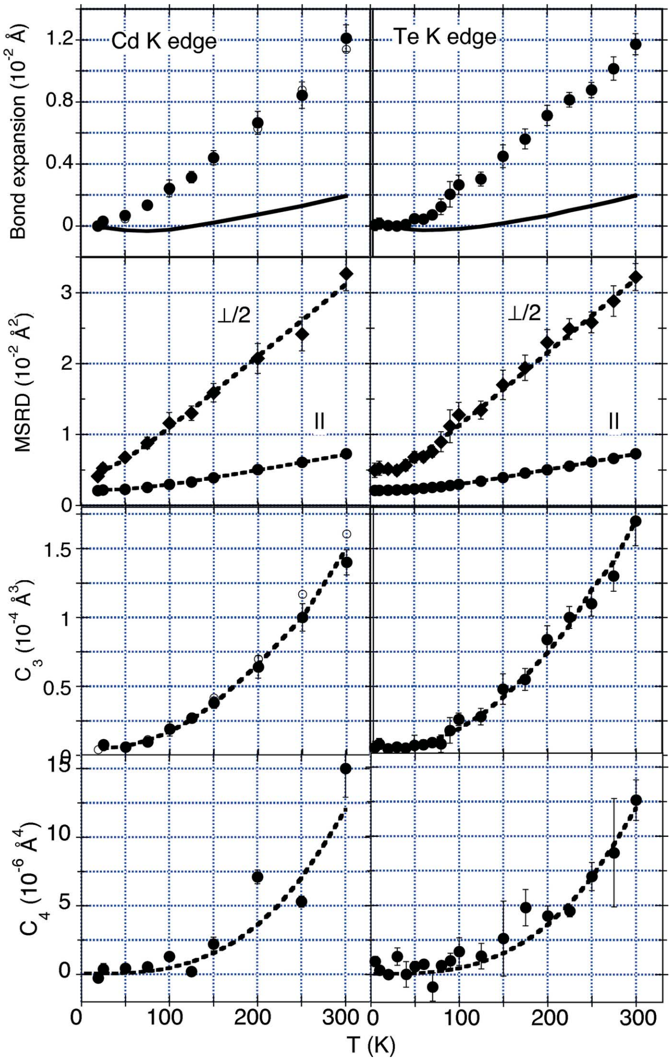

Figure 6

Results of the first-shell analysis for CdTe. Left-hand and right-hand panels refer to the Cd and Te edges, respectively. Top row: bond thermal expansion from EXAFS (full circles from the ratio method, open circles from non-linear fitting) and from Bragg diffraction and dilatometry (continuous line). Second row: parallel MSRD $\Delta u_\parallel^2$ (circles) and halved perpendicular MSRD $\Delta u_\perp^2/2$ (diamonds); the dashed lines are the best-fitting Einstein models. Third row: third cumulant (full circles from the ratio method, open circles from non-linear fitting); the dashed line is the best fit by equation (5). Bottom row: fourth cumulant; the dashed line is the best fit by equation (6).

with respect to the first effective cumulants δC_1 ($\sim 0.06 \times 10^{-2}$ Å).

3.2.2. Non-linear best fit. In the second procedure, back-scattering amplitudes, phase shifts and inelastic terms were calculated by the *FEFF6* code (Rehr *et al.*, 1992; Ankudinov *et al.*, 1998) and a non-linear best fit of calculated to experimental spectra was then performed by the *IFEFFIT* code (Newville, 2001) using the graphical interface *Artemis* (Ravel & Newville, 2005).

The values of e_0 (mismatch between theoretical and experimental origin of k scales) and S_0^2 (amplitude reduction factor) were left free in a first trial analysis; average values were then calculated and maintained fixed in a further analysis. To allow a direct comparison with the results from the ratio method, the relative values of cumulants were calculated by taking the lowest temperature as a reference.

The non-linear fit approach allowed us also to check the possible leakage of longer scattering paths on the first-shell contribution (see below).

4. Results

The main results of the first-shell analysis are summarized in Fig. 6. The results from the Cd *K*-edge (left-hand panels) can be directly compared with the results from the Te *K*-edge (right-hand panel). Some significant parameters are listed in Table 2.

The top plots in Fig. 6 show the relative values of the first cumulant δC_1^* of the real distribution, corresponding to the bond thermal expansion: full circles and open circles are from the ratio method and from *FEFFIT*, respectively. The continuous line is the bond expansion δR_c proportional to the lattice expansion measured by Bragg diffraction or dilatometric techniques (Touloukian *et al.*, 1977). The difference between the two thermal expansions corresponds to the temperature variation of the perpendicular MSRD (Fornasini, 2001),

$$\delta C_1^* - \delta R_c = \delta \langle \Delta u_\perp^2 \rangle / 2R_c. \tag{4}$$

To check the possible effects due to the leakage of the outer-shells contributions on the first-shell signal, an alternative analysis was performed on the filtered signal including the single-scattering contributions of the first three coordination shells and the most relevant multiple-scattering paths (Fourier back-transform from 1.6 to 5.7 Å in Fig. 3). The results for the first cumulant at the Cd *K*-edge are summarized in Fig. 7, where solid circles and open symbols are from the ratio method and the non-linear fitting procedures, respectively. Open circles refer to the analysis of the filtered first-shell signal (as in Fig. 6) made with a fixed energy shift e_0 = 3.4 eV, obtained as the average value over a first trial analysis. Open triangles refer to the analysis of the signal including the first three shells and the relevant MS paths: up triangles for e_0 = 3.4 eV, as for the analysis limited to the first shell, down triangles for e_0 = 4.5 eV, obtained as the average value over a first trial analysis. Fig. 7 suggests that leakage effects are negligible for the case of CdTe.

This conclusion cannot be simply generalized to other systems. Leakage effects cannot be *a priori* excluded by a

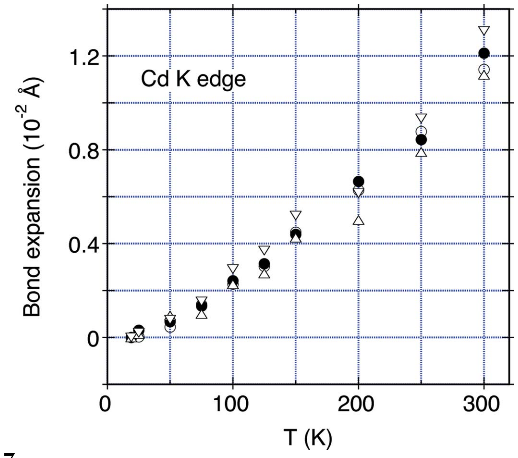

Figure 7
Comparison of nearest-neighbours bond expansions from different procedures of Cd *K* EXAFS analysis: ratio method (full circles) and non-linear fit (open symbols), limited to the first shell (open circles), including the second and third shells (up and down triangles) for two different e_0 values. The uncertainty bars have been omitted for clarity.

simple visual inspection of the Fourier transform plots. Non-linear fitting including outer coordination shells is not necessarily a conclusive check, since its reliability can be affected by the evaluation of multiple-scattering effects and by correlation effects. Besides, in case of discrepancy, no obvious reference for calibration is at disposal, in view of the difference between bond and lattice thermal expansions (see below, §5.3). Leakage effects have been found to be significant when the nearest neighbour (first shell) is a relatively weak scatterer and the next nearest neighbour (second shell) is a relatively strong scatterer as in InP (Schnohr, 2012).

The plots in the second row in Fig. 6 represent the parallel MSRD $\langle \Delta u_{\parallel}^2 \rangle$ and the halved perpendicular MSRD $\langle \Delta u_{\perp}^2 \rangle/2$ (projected along one direction for example). The relative values of the parallel MSRD correspond to the relative values of the second cumulant δC_2^*; the relative values of the perpendicular MSRD have been obtained from equation (4). Absolute values of both parallel and perpendicular MSRDs have been evaluated by fitting correlated Einstein models to the temperature dependence of the experimental relative values (Vaccari & Fornasini, 2006). The corresponding Einstein frequencies are listed in Table 2. The agreement between the Cd and Te results is very good. The second cumulants of the real and effective distributions, C_2^* and C_2, respectively, are connected by equation (3); the Einstein frequencies for the effective distribution are 1% higher than for the real distribution.

The plots in the third row in Fig. 6 represent the third cumulants C_3^*. The absolute values have been evaluated by fitting the quantum perturbative model (Frenkel & Rehr, 1993; Yokoyama, 1999),

$$C_3^* \simeq -\frac{2k_3\sigma_0^4}{k_0}\,\frac{z^2+10z+1}{(1-z)^2}, \qquad (5)$$

to the experimental relative values. In equation (5), $\sigma_0^2 = \hbar/2\mu\omega$, $z = \exp(-\beta\hbar\omega)$, $\omega = (k_0/\mu)^{1/2}$, μ is the reduced mass, and $\omega = 2\pi\nu_{\parallel}$ and k_0 are the Einstein angular frequency and the force constant determined from the second cumulant. The visual agreement between the Cd and Te values can be considered to be quite good. A quantitative evaluation is given by the parameters listed in Table 2. The 8% discrepancy between the Cd and Te values of the force constant k_3 is larger than the combined error bars. The discrepancy is instead consistent with the error bars for the asymptotic zero Kelvin values. In the previous paper (Abd el All *et al.*, 2012), the force constants k_0 and frequencies ω best fitting the second cumulant C_2 of the effective distribution were used in (5) (instead of the second cumulant C_2^* of the real distribution), so that slightly different values of k_3 were quoted (-2.09 and -2.17 eV Å^{-3}).

The lower plots in Fig. 6 represent the fourth cumulants C_4^*. The best fit of the Te data with the quantum perturbative model (Yokoyama, 1999)

$$\begin{aligned} C_4^* = & -\frac{12\,k_4\sigma_0^8}{\hbar\omega}\,\frac{z^3+9z^2+9z+1}{(1-z)^3} \\ & -\frac{144\,k_4\sigma_0^8}{k_{\rm B}T}\,\frac{z^2}{(1-z)^4} \\ & +\frac{12\,k_3^2\sigma_0^{10}}{(\hbar\omega)^2}\,\frac{5z^3+109z^2+109z+5}{(1-z)^3} \\ & +\frac{720\,k_3^2\sigma_0^{10}}{\hbar\omega k_{\rm B}T}\,\frac{z^2}{(1-z)^4} \end{aligned} \qquad (6)$$

(dashed line) gives a fourth-order force constant $k_4 = (-0.36 \pm 0.03)$ eV Å^{-4} and a zero point value 0.2×10^{-6} Å^4. The model best fitting the Te data is consistent with the Cd data.

5. Discussion

5.1. Uncertainty evaluation

A sound assessment of the uncertainty of EXAFS results requires a careful evaluation of random fluctuations and systematic errors in both experimental and data analysis procedures.

The influence of counting statistics is generally negligible in transmission measurements at third-generation synchrotron radiation sources. A number of other factors, however, should be taken into account: temperature fluctuations of the sample; temperature fluctuations and mechanical instabilities of monochromator, mirrors and their supports; calibration and resolution of the monochromator angular encoder; electron beam fluctuations. All these factors can lead to non-negligible uncertainties of the photon energy and, on a non-perfectly homogeneous sample, to variations of the amplitude of EXAFS, not to mention possible systematic errors, related for example to the sample temperature calibration, photon beam energy calibration, sample deterioration, and so on.

Not all of these factors can reasonably be under complete control of the synchrotron radiation users or even of the beamline scientists. Suitable experimental strategies and data analysis procedures, joined to a critical discussion of results, can lead to a sound *a posteriori* evaluation of uncertainties and of their most relevant causes.

As a general rule of experimental practice, EXAFS measurements under given conditions (*e.g.* on a given sample at a given temperature) should be repeated a convenient number of times, typically at least three times. When this happens, the different spectra are frequently summed to obtain an average EXAFS function $\chi(k)$. We consider it preferable to analyse each spectrum separately. The resulting cumulants represent a restricted sample of a parent population of values generated by short-term fluctuations. It is reasonable to account for these fluctuations by evaluating the uncertainty as the standard deviation of the distribution of mean values; this contribution to uncertainty decreases when the number of spectra increases.

As a numerical example, let us consider the phase analysis of seven files measured at 300 K at the Te K-edge and compared with the average reference file at 20 K (Fig. 5, dashed lines). For the fitting interval k = 4–14 Å^{-1}, the values of the odd cumulants of the effective distribution were ΔC_1 = (0.73 ± 0.04) × 10^{-2} Å and ΔC_3 = (1.65 ± 0.11) × 10^{-4} Å^3.

A second source of uncertainty is connected to the data analysis procedure. Different windows and k weights in Fourier transform and back-transform, as well as different fitting intervals in k-space, lead to different values of cumulants. In this respect the ratio method, based on the separate analysis of phases and amplitudes, is far less affected by statistical correlation effects than the non-linear fitting procedures. The different values of cumulants obtained by different choices of data analysis parameters cannot be considered as independent samples of a parent distribution: increasing the number of fitting intervals cannot decrease the final uncertainty. The different values can be considered as sampling a uniform distribution, and the corresponding uncertainty can be evaluated as the standard deviation of the distribution, $\sigma_n = \Delta(\delta C_n)/(12)^{1/2}$. The point here is not the repetition of the fitting procedure over a large number of fitting intervals but a sound choice of the width $\Delta(\delta C_n)$ of the uniform distribution, which in turn depends on the choice of the extrema $k_{\rm min}$ and $k_{\rm max}$ of the fitting intervals. In the ratio method the largest fitting interval can be chosen as the interval where the phase differences (Fig. 5) or the logarithms of amplitudes ratios (Fig. 4) of different files measured under the same conditions show a reasonable agreement. The visual choice suffers from some arbitrariness, but leads generally to quite conservative estimates of uncertainty, in view of the large sensitivity of the phase and amplitude plots to tiny discrepancies of the spectra.

As a numerical example, let us consider again the phase analysis of the seven files measured at 300 K at the Te K-edge (Fig. 5, dashed lines) and focus on the first cumulant. The three fitting intervals from $k_{\rm min}$ = 4 to $k_{\rm max}$ = 13, 14 or 15 Å^{-1} give different average values of the first cumulants ΔC_1 = 0.678, 0.73 and 0.8 × 10^{-2} Å; the contribution to the total uncertainty is 0.035 × 10^{-2} Å.

An important contribution to the evaluation of uncertainty is represented by the comparison of independent measurements performed on the same system, for example in different laboratories or on samples of different thicknesses and possibly at two different absorption edges. From Fig. 6 one can appreciate the extent of the differences between the measurements performed on different edges, at two different beamlines, in different times, on samples with different thicknesses.

A last point for the evaluation of the quality of results is the comparison of the temperature dependence of the cumulants with a reasonably smooth behaviour. An interesting example is given by the sequence of cumulants obtained from the Te and Cd edges between 50 and 150 K (Fig. 6). In the right-hand panels of Fig. 6 (Te K-edge) the quantities derived from the phase analysis (odd cumulants and perpendicular MSRD) are characterized by a tiny deviation from the expected smooth temperature dependence; this effect is absent in the left-hand panels of Fig. 6 (Cd K-edge). In the present case the discrepancies between the results from Te and Cd edges are consistent with the uncertainty bars: one can reasonably assume that, had a larger number of spectra been measured at each temperature, the Te data would have been in better agreement with a smooth temperature dependence. We cannot, however, exclude the possibility that the observed kinks are due to long-period fluctuations of the experimental apparatuses or to occasional systematic errors, which escaped our direct detection anyway; in such a case they can be considered as a measure of the extent of long-term reproducibility of a routine experiment performed on a standard beamline.

5.2. Comparisons with theoretical models

The agreement between the results from EXAFS measured at two different edges and the smooth temperature dependence of cumulants are internal self-consistency experimental checks. External accuracy checks can rely on the comparison of experimental results with theoretical models.

The simplest approach consists of comparing the temperature dependence of structural and dynamical quantities from EXAFS with parametrized models, for example the correlated Einstein or the correlated Debye models for the parallel and perpendicular MSRDs (Vaccari & Fornasini, 2006) and more refined anharmonic models, such as equations (5) and (6) for high-order cumulants (Frenkel & Rehr, 1993; Yokoyama, 1999). The agreement of experimental data with parametrized models is generally a good check that there are no significant systematic experimental errors and that the cumulant series converges fast enough, so that the polynomial coefficients $\tilde{C}_n$ are good approximations of the corresponding cumulants C_n^* (Dalba *et al.*, 1993). A non-negligible disagreement could be attributed to different causes, such as the low quality of experimental data, the non-convergence of the cumulant series and the presence of phase transitions. The evaluation of the soundness of experimental cumulants through a comparison of their temperature dependence with theoretical models is a sensible practice, in view of the relatively limited range of validity of the cumulant expansion (Crozier *et al.*, 1988; Dalba *et al.*, 1993; Filipponi, 2001).

The Einstein and Debye models are different at low temperatures, owing to the different approximations to the density of vibrational states (VDOS), the Debye VDOS being in principle more realistic. The difference can, however, be barely appreciated when fitting to experimental data, in view of the data uncertainty and of the anharmonicity contributions. The Debye model is recommended for monatomic Bravais crystals, for which the Debye temperature is very similar for the different coordination shells and comparable with the Debye temperatures from other techniques (Fornasini *et al.*, 2004). For non-Bravais crystals the Debye temperatures can be very different for different coordination shells. The Einstein frequencies are different for different coordination shells too; an advantage of the Einstein model is that the Einstein frequencies are directly connected to effective force constants, $k_0 = 4\pi^2\mu\nu_{\parallel}^2$, which measure the effective strength of the bond between absorber and backscatterer atoms. The discrepancy between the best-fitting Einstein model and the MSRDs calculated by dynamical simulations on different crystalline structures has been estimated recently (Sanson, 2008), and found to be no larger than 5% and 10% for the parallel and perpendicular MSRDs, respectively.

The comparison of the third and fourth cumulants with the quantum perturbative models of equations (5) and (6) is a more refined test. For CdTe, the agreement is good for the third cumulant, and satisfactory for the fourth (Fig. 6).

Full lattice dynamical calculations (Baroni *et al.*, 2001) in harmonic approximation can in principle reproduce the MSRDs, both parallel (Beni & Platzman, 1976; Strauch *et al.*, 1996) and perpendicular (Vaccari & Fornasini, 2006), provided a good evaluation of the phase relations between eigenvectors of the dynamical matrix is achieved. Anharmonicity effects (including third cumulant and anharmonic corrections to the MSRDs) can be obtained by a perturbative approach (Birner *et al.*, 2001).

Classical molecular dynamics (MD) simulations intrinsically take into account anharmonicity. The high-temperature behaviour of the EXAFS cumulants has been well reproduced for copper (Edwards *et al.*, 1997), germanium (Sanson, 2010) and CdSe (Sanson, 2011). Classical MD, however, cannot reproduce low-temperature quantum effects caused by zero-point energy in thermal expansion, MSRDs and the third cumulant. A purely classical treatment of the experimental third cumulant, supported by classical MD calculations, can lead to subtle inconsistencies in the analysis and interpretation of EXAFS results. An interesting example is the negative shift of the effective pair potential when temperature increases, hypothesized for AgI and CdSe to explain the results of the classical treatment (Dalba *et al.*, 1994, 1998; Sanson, 2011).

More effective, though more complex, approaches, rely on *ab initio* MD (Vila *et al.*, 2012) or on the path-integral technique, based on Monte Carlo sampling (PIMC) or on the use of an effective classical potential (Miyanaga *et al.*, 2000). A good reproduction of the experimental data for copper has been obtained by PIMC (a Beccara *et al.*, 2003; a Beccara & Fornasini, 2008), including the perpendicular MSRD and the relation between the third cumulant and thermal expansion (see below).

5.3. EXAFS and crystallographic distances

The ratio method only gives relative values of the first-shell cumulants with respect to the reference temperature. In principle, absolute values can be obtained by a non-linear fit of simulated spectra to the experimental ones (Rehr *et al.*, 1992; Ankudinov *et al.*, 1998; Newville, 2001). However, the accuracy of the absolute values of distances and Debye–Waller factors critically depends on the accuracy by which backscattering amplitudes, phase shifts and inelastic terms are calculated, and can be assessed only by comparison with known standards.

The comparison with standards is far from trivial concerning the nearest-neighbours bond distance, in view of the non-negligible difference between EXAFS and crystallographic values $C_1^* = \langle r\rangle$ and R_c, respectively,

$$C_1^* = R_c + \langle\Delta u_\perp^2\rangle/2R_c. \qquad (7)$$

A calibration of EXAFS simulations against crystallographic distances can be misleading if accuracies of the order of some 0.001 Å are sought (Chantler *et al.*, 2012*a*).

The ratio method allows a direct evaluation of the temperature dependence of the bond distance, without reference to the crystallographic distance. In the top row of Fig. 6, the variations δC_1^* and δR_c, independently measured, are compared assuming a common zero value for T = 0 K. Once the absolute values of the perpendicular MSRD have been estimated by the best-fitting Einstein model (Fig. 6, second row), the difference between EXAFS and crystallographic bond distances can be calculated through equation (4). Fig. 8 shows that the difference for CdTe is of the order of 0.002 Å at low temperatures and increases up to 0.011 Å at 300 K. The discrepancy between EXAFS and crystallographic distances depends on the intensity of relative vibrations perpendicular

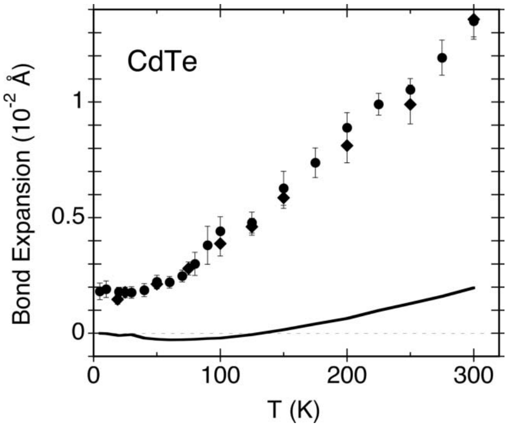

Figure 8
Bond expansion measured by EXAFS (circles and diamonds are from Te and Cd edges, respectively) compared with the crystallographic bond expansion (continuous line). The zero of the vertical axis has been arbitrarily set in correspondence of the crystallographic bond length at 0 K.

Table 3
Difference $C_1^* - R_c$ (in Å) between the nearest-neighbours bond distance measured by EXAFS and by Bragg diffraction for Cu (Fornasini *et al.*, 2004), Ge (Dalba *et al.*, 1999) and CdTe (present paper).

T (K)	Cu	Ge	CdTe
5	1.3×10^{-3}	1.5×10^{-3}	1.8×10^{-3}
300	4×10^{-3}	8×10^{-3}	11.5×10^{-3}

to the bond. Three different situations are compared in Table 3 in order of increasing intensity of perpendicular vibrations: copper (Fornasini *et al.*, 2004), germanium (Dalba *et al.*, 1999) and CdTe (present).

5.4. Third cumulant

The inclusion of the third cumulant in the analysis of the first shell is necessary to obtain reliable information on distances. As an example, let us consider a typical plot of phase differences, such as Fig. 5: neglecting the third cumulant corresponds to fitting the phase difference with a horizontal straight line. In the case of CdTe at 300 K this would correspond to underestimating the difference in nearest-neighbour distances between 300 and 0 K by about 0.003 Å (assuming a fit interval from 4 to 13 Å^{-1}). The error decreases when the temperature is lowered.

The third cumulant measures the asymmetry of the distribution of distances, which is connected to the asymmetry of the effective pair potential. Contrary to the case of two-atomic molecules, it has been experimentally observed that in many atomic systems the expansion of the nearest-neighbour distance is not completely accounted for by the asymmetry of the effective pair potential (Dalba *et al.*, 1999; Fornasini *et al.*, 2004; Vaccari *et al.*, 2007; Abd el All *et al.*, 2012; Yokoyama & Eguchi, 2011). An additional rigid shift of the effective pair potential with temperature has to be assumed in order to reproduce the expansion measured by the first cumulant.

The presence of a rigid shift of the maximum of the distance distribution, corresponding to the minimum of the effective pair potential, has been confirmed for Cu by path-integral Monte Carlo simulations (a Beccara & Fornasini, 2008) and for Ge by MD simulations (Sanson, 2010). In both cases the simulations further show that the contribution of the potential asymmetry to thermal expansion is much smaller for the outer shells than for the first shell. The outer-shell distributions are to a good approximation Gaussian, and the thermal expansion of their average distances is accounted for mainly by their rigid shift. In conclusion, no reliable information on thermal expansion can be obtained from the third cumulant. From a practical point of view, the reduced asymmetry of the outer-shells distributions suggests that the inclusion of the third cumulant, which is mandatory for accurate first-shell analyses, is much less important for the outer shells.

6. Conclusions

The evaluation of the accuracy of temperature-dependent EXAFS measurements performed at standard synchrotron radiation beamlines has been discussed with reference to the results of a recent experiment on CdTe, where the Cd and Te edges have been independently measured at different beamlines.

Attention has been focused on the relative values of the first four cumulants of the nearest-neighbour distribution of distances. The analysis has been performed by both the ratio method and the non-linear fit procedure based on the *FEFFIT* software: the results of the two methods are in good agreement. The non-linear fit procedure has allowed us to check that the leakage of longer paths on the first-shell contribution is negligible for the present case of CdTe.

The accuracy of experimental results has been evaluated by separately considering the contributions of the differences between repeated measurements at the same temperature and the different data analysis procedures (including different fitting intervals). The results from the Cd and Te edges are in good agreement up to the fourth cumulant and consistent with a smooth temperature dependence of cumulants.

A difference between EXAFS and crystallographic nearest-neighbour distances of about 1.8×10^{-3} Å at 5 K and 11.5×10^{-3} Å at 300 K was found. These differences are larger than the differences previously found for Cu and Ge.

Possibilities and limitations of accuracy checks based on the comparison of experimental results with theoretical predictions have been discussed on general grounds, including the relative merits of the phenomenological Einstein and Debye models as well as of the molecular dynamics and of more sophisticated simulation techniques based on path-integral methods.

The European Synchrotron Radiation Facility (ESRF) is acknowledged for provision of synchrotron radiation facilities. This work was partially supported by the ESRF project HS-3603.

References

Abd el All, N., Dalba, G., Diop, D., Fornasini, P., Grisenti, R., Mathon, O., Rocca, F., Thiodjio Sendja, B. & Vaccari, M. (2012). *J. Phys. Condens. Matter*, **24**, 115403.

a Beccara, S., Dalba, G., Fornasini, P., Grisenti, R., Pederiva, F., Sanson, A., Diop, D. & Rocca, F. (2003). *Phys. Rev. B*, **68**, 140301.

a Beccara, S. & Fornasini, P. (2008). *Phys. Rev. B*, **77**, 172304.

Ankudinov, A. L., Ravel, B., Rehr, J. J. & Conradson, S. D. (1998). *Phys. Rev. B*, **58**, 7565.

Ascone, I., Asakura, K., George, G. N. & Wakatsuki, S. (2012). *J. Synchrotron Rad.* **19**, 849–850.

Baroni, S., de Gironcoli, S. & Dal Corso, A. (2001). *Rev. Mod. Phys.* **73**, 515–562.

Beni, G. & Platzman, P. M. (1976). *Phys. Rev. B*, **14**, 1514–1518.

Birner, G., Strauch, D. & Pavone, P. (2001). Unpublished.

Bunker, G. (1983). *Nucl. Instrum. Methods Phys. Res.* **207**, 437–444.

Chantler, C. T., Barnea, Z., Tran, C. Q., Rae, N. A. & de Jonge, M. D. (2012*a*). *J. Synchrotron Rad.* **19**, 851–862.

Chantler, C. T., Islam, M. T., Rae, N. A., Tran, C. Q., Glover, J. L. & Barnea, Z. (2012*b*). *Acta Cryst.* A**68**, 188–195.

Chantler, C. T., Tran, C. Q., Barnea, Z., Paterson, D., Cookson, D. J. & Balaic, D. X. (2001). *Phys. Rev. A*, **64**, 062506.

Crozier, E. D., Rehr, J. J. & Ingalls, R. (1988). In *X-ray Absorption*, edited by D. C. Koningsberger & R. Prins, ch. 9, pp. 373–442. New York: John Wiley & Sons.

Dalba, G., Fornasini, P., Gotter, R., Cozzini, S., Ronchetti, M. & Rocca, F. (1994). *Solid State Ion.* **69**, 13–19.

Dalba, G., Fornasini, P., Grisenti, R., Pasqualini, D., Diop, D. & Monti, F. (1998). *Phys. Rev. B*, **58**, 4793–4802.

Dalba, G., Fornasini, P., Grisenti, R. & Purans, J. (1999). *Phys. Rev. Lett.* **82**, 4240–4243.

Dalba, G., Fornasini, P. & Rocca, F. (1993). *Phys. Rev. B*, **47**, 8502–8514.

Edwards, A. B., Tildesley, D. J. & Binsted, N. (1997). *Mol. Phys.* **91**, 357–369.

Filipponi, A. (2001). *J. Phys. Condens. Matter*, **13**, R1–R38.

Fornasini, P. (2001). *J. Phys. Condens. Matter*, **13**, 7859–7872.

Fornasini, P. (2008). *The Uncertainty in Physical Measurements*. New York: Springer.

Fornasini, P., a Beccara, S., Dalba, G., Grisenti, R., Sanson, A., Vaccari, M. & Rocca, F. (2004). *Phys. Rev. B*, **70**, 174301.

Frenkel, A. I. & Rehr, J. J. (1993). *Phys. Rev. B*, **48**, 585–588.

Glover, J. L., Chantler, C. T., Barnea, Z., Rae, N. A. & Tran, C. Q. (2010). *J. Phys. B*, **43**, 085001.

Miyanaga, T., Suzuki, T. & Fujikawa, T. (2000). *J. Synchrotron Rad.* **7**, 95–102.

Newville, M. (2001). *J. Synchrotron Rad.* **8**, 322–324.

Pettifer, R. F., Mathon, O., Pascarelli, S., Cooke, M. D. & Gibbs, M. R. (2005). *Nature (London)*, **435**, 78–81.

Prestipino, C., Mathon, O., Hino, R., Beteva, A. & Pascarelli, S. (2011). *J. Synchrotron Rad.* **18**, 176–182.

Purans, J., Afify, N. D., Dalba, G., Grisenti, R., De Panfilis, S., Kuzmin, A., Ozhogin, V. I., Rocca, F., Sanson, A., Tiutiunnikov, S. I. & Fornasini, P. (2008). *Phys. Rev. Lett.* **100**, 055901.

Ravel, B. & Newville, M. (2005). *J. Synchrotron Rad.* **12**, 537–541.

Rehr, J. J., Albers, R. C. & Zabinsky, S. I. (1992). *Phys. Rev. Lett.* **69**, 3397–3400.

Sanson, A. (2008). *J. Synchrotron Rad.* **15**, 514–518.

Sanson, A. (2010). *Phys. Rev. B*, **81**, 012304.

Sanson, A. (2011). *J. Phys. Condens. Matter*, **23**, 315401.

Schnohr, C. (2012). Private communication.

Steinmann, R. & van der Linden, P. (2006). *Proceedings of the International Worskshop on Mechanical Engineering Design of Synchrotron Radiation Equipment and Instrumentation (MEDSI 2006)*, 24–26 May 2006, Hyogo, Japan.

Strauch, D., Pavone, P., Nerb, N., Karch, K., Windl, W., Dalba, G. & Fornasini, P. (1996). *Physica B*, **219**/**220**, 436–438.

Touloukian, Y. S., Kirby, R. K., Taylor, R. E. & Desai, P. D. (1977). *Thermophysical Properties of Matter*, Vol. 13. New York: Plenum.

Vaccari, M. & Fornasini, P. (2006). *J. Synchrotron Rad.* **13**, 321–325.

Vaccari, M., Grisenti, R., Fornasini, P., Rocca, F. & Sanson, A. (2007). *Phys. Rev. B*, **75**, 184307.

Vila, F. D., Lindahl, V. E. & Rehr, J. J. (2012). *Phys. Rev. B*, **85**, 024303.

Yokoyama, T. (1999). *J. Synchrotron Rad.* **6**, 323–325.

Yokoyama, T. & Eguchi, K. (2011). *Phys. Rev. Lett.* **107**, 065901.